Journal of Intelligent Systems and Internet of Things
Vol. 17, No. 02, PP. 392-403, 2025
DOI: https://doi.org/10.54216/JISIoT.170225

Deep Learning-Based BER Enhancement for 64x64 MIMO-FSO NOMA Systems Under Various Atmospheric Turbulence Senarios

Hasan Farooq Radeef[1,3,*], Lwaa F. Abdulameer[2]

[1]Electronic and communication Department, Institute of Laser for Postgraduate Studies, University of Baghdad, Baghdad, Iraq

[2]Department of Information and Communication, Al-khwarizmi College of Engineering, University of Baghdad, Iraq

[3]Department of Computer Networks, Information College of Engineering, Al-Nahrain University, Iraq

Emails: hasan.ahmed2101p@ilps.uobaghdad.edu.iq; lwaa@kecbu.uobaghdad.edu.iq

Abstract

The current exponential growth in the demand for bandwidth is the most urgent challenge for next-generation wireless systems. One of the most appropriate techniques to overcome this situation is Free-space optical (FSO) communication due to the provision of an ample bandwidth. The main disadvantage of FSO communication systems is that the optical beam, propagating through atmospheric turbulence, can be distorted to an unacceptable level. In this work, a 64x64 MIMO-FSO system with Non-Orthogonal Multiple Access (NOMA) and QPSK modulation scheme is assessed. We compare the Bit Error Rate (BER) performance of the system under 4 theoretical turbulence channel models: Log-Normal, Gamma-Gamma, Fisher-Snedecor, Negative Exponential, as well as 4 real seasonal LogCn² datasets. Classical Maximum Likelihood (ML) detection was compared against the deep learning-based ML detection using a Deep Neural Network (DNN) as well as an Autoencoder model. We found that the autoencoder model has outperformed the classical ML detection in terms of BER performance, especially for the weaker user, when NOMA is considered. It was also found that using real datasets that represent real turbulence conditions the proposed system is highly effective and can serve as intelligent fronthaul/backhaul solutions for dense IoT networks such as smart cities, autonomous vehicles, and industrial automation.

Received: January 23, 2025 Revised: March 28, 2025 Accepted: June 12, 2025

Keywords: Massive MIMO; FSO; DNN; IoT; Intelligent Systems

1. Introduction

The high demand for wireless data has exceeded the capacity of traditional radio frequency (RF) systems. Free-space optical (FSO) communication has been explored as a promising supplement due to its advantages such as high data rates, license-free spectrum, and physical layer security. However, FSO transmissions are prone to atmospheric impairments such as turbulence, scintillation, and pointing errors that deteriorate the system performance. MIMO techniques have been implemented to enhance the link performance under fading with spatial diversity gains. Non-Orthogonal Multiple Access (NOMA) is another technique to improve the spectral efficiency of the systems by serving multiple users over the same frequency and time resource [1-3].

The conventional detection schemes such as Maximum Likelihood (ML) have been proven to perform poorly in severe fading conditions, especially for NOMA users with low power allocation. Deep learning (DL) methods have recently been proposed to improve the symbol detection and channel estimation in complicated wireless systems. In this paper, we study the incorporation of DL approaches to the 64x64 MIMO-FSO NOMA system

with QPSK modulation under theoretical and experimental turbulence channels. The DL techniques, which include DNN and Autoencoders, are evaluated with benchmark ML techniques for their symbol detection performance.

The paper investigates a massive MIMO-FSO system (64×64 apertures) that uses non-orthogonal multiple access (NOMA) and QPSK modulation. Key contributions include:

i. **Comprehensive BER evaluation under multiple turbulence models:** The authors simulate the 64×64 MIMO-FSO-NOMA system using four theoretical turbulence models (log-normal, gamma–gamma, Fisher–Snedecor and negative exponential) and four real seasonal log-Cn^2 data sets. This provides insight into system performance across weak, moderate and severe turbulence conditions.

ii. **Comparison of classical and deep-learning-based receivers:** Three detection schemes are considered: a conventional maximum-likelihood detector, a deep neural network channel estimator, and an autoencoder that jointly learns the transmitter and receiver. The study shows that the autoencoder consistently achieves lower BER than maximum-likelihood detection across all channel models, especially for the weaker NOMA user, because it learns to mitigate interference and turbulence jointly. The DNN-based detector also outperforms the conventional detector by learning channel statistics and improving symbol recovery.

iii. **Focus on large-scale MIMO and NOMA:** By employing a 64×64 transceiver array, the paper explores massive MIMO-FSO with NOMA for two users. Power allocation is set following NOMA policy (e.g., 0.8 for the strong user and 0.2 for the weak user). The results show that even with massive spatial diversity, classical detection struggles under severe turbulence, highlighting the need for machine-learning-based approaches.

iv. **Use of QPSK modulation:** While many FSO studies use on–off keying or BPSK, this work utilises QPSK to achieve higher spectral efficiency. The study demonstrates that deep-learning receivers can handle the increased complexity of QPSK in turbulent FSO channels.

v. **Evaluation using real turbulence data:** Using real seasonal log-Cn^2 data sets, the authors show that BER performance varies by season. The system performs better in summer and autumn than in winter and spring, as the latter have stronger atmospheric turbulence. This highlights the practicality of the proposed system for real-world FSO links.

vi. **Implications for future FSO systems:** The results indicate that integrating deep learning with massive MIMO-FSO and NOMA can significantly improve BER performance under diverse turbulence conditions, making FSO a more viable option for high-capacity future networks. The work provides a foundation for further research on end-to-end learning and adaptive power allocation in optical wireless systems.

Overall, the paper extends existing literature by evaluating deep-learning receivers in a massive MIMO-FSO-NOMA system with realistic turbulence models and QPSK modulation, demonstrating that autoencoders offer substantial BER gains over traditional detection methods.

Table 1 presents the latest research on ML integration in FSO systems. The literature review focused on the most recent studies.

Table 1: Related research

[4]	Anand Kumar et al., 2021	Analysed the bit error rate of MIMO-FSO with respect to gamma-gamma distributed turbulence channel. They proposed a mathematically tractable power series-based probability density function (PDF) of gamma-gamma fading with pointing errors and atmospheric turbulence.
[5]	Maged A. Esmail et al., 2021	Focused on three aspects in FSO: amplified spontaneous emission noise, turbulence and pointing errors. They then compared the system performance of support vector machine and CNN.
[6]	Lepuri Jathin Sravan Kumar et al., 2022	Proposed a decoding technique for decoding on–off keying modulated FSO signals using support vector machines, tested under various atmospheric weather conditions such as fog, rain and snow, as well as turbulence, and pointing errors. Simulated numerical results demonstrate that the proposed SVM-based decoding schemes can mitigate attenuation, pointing error and turbulent channel impairments.

[7]	Manon P. Bart et al., 2022	Reduced the BER in FSO communication by presenting and experimentally validating a CNN through a post-processing approach that is significantly simpler and cheaper than existing solutions based on advanced optics.
[8]	S.A. Abd El-Mottaleb et al., 2022	Examined K-nearest and support vector machine algorithms under four different weather conditions for FSO spectral amplitude coding optical code division multiple access communication system including simulation results Q-factor, BER and SNR.
[9]	Shagufta Henna et al., 2023	Studied deep reinforcement learning to improve the capacity of the hybrid FSO/RF system.
[10]	M.A. Esmail, 2023	Used ML to monitor the amount and type of distortion in the optical channel and used Gaussian process regression as an ML technique to predict turbulence, OSNR and chromatic dispersion (CD), which are the main channel impairments that arise in hybrid all-optical fibre/FSO channels. The model can better predict various impairments, but the performance accuracy degrades under strong amplified spontaneous emission noise, where the model demonstrated lower accuracy in predicting light turbulence parameters.
[11]	L. Antonios et al., 2023	Used ML to estimate and model the refractive index structure parameter by using six regression algorithms.
[12]	Somia A. Abd El-Mottaleb et al., 2024	Utilised ML for SISO/MIMO-FSO channel classification and focused on system performance under different fog conditions.
[13]	Al-Imran et al., 2024	Considered atmospheric turbulence channels for estimating the channel coefficient matrix of a massive MIMO-FSO communication system. This advanced model leverages attention mechanisms to focus on relevant features and residual connections to facilitate better gradient flow, addressing the vanishing gradient problem and enabling the learning of complex features. From the MSE performance
[14]	Ashenafi Paulos Forsidoet al., 2025	Investigated FSO transmission in various weather conditions under different modulation formats and ML models. They used various ML algorithms to determine BER over SNR and received power for OOK–NRZ and QPSK modulated signals in a WDM-FSO system. ML enhanced system performance and reduced BER due to its adaptability.

2. System Model

MIMO-FSO system equipped with 64 × 64 transceiver is proposed and simulated over different channel models. For the purpose of modulation, quadrature phase-shift keying (QPSK) modulation is chosen due to its low complexity and better reliability. NOMA users are allocated power coefficient (PNOMA) such that, PNOMA (1) > PNOMA(2). It is always so that the strong user (User 1) is assigned a higher power than weak user (User 2) as per NOMA standard policy.

The system is simulated over the following channel models:

Lognormal: This channel model is used to represent the weak to moderate turbulence range where σ (variance) = 0.3. Lognormal PDF can be rewritten as [15]

$$f(I) = \frac{1}{2\sqrt{2\pi\sigma_x^2 I}} exp\left[-\frac{(ln(I)-\mu)^2}{8\sigma_x^2}\right] \quad (1)$$

Gamma-Gamma: This channel model is used to consider the small-scale fading as well as large scale fading phenomena with α = 3.0 and β = 2.0. with its PDF given by [15]

$$f_I(I) = \frac{2(\alpha\beta)}{\Gamma(\alpha)\Gamma(\beta)} I^{(\frac{\alpha+\beta}{2})-1} K_{\alpha-\beta}(2\sqrt{\alpha\beta I}),\ I > 0 \quad (2)$$

In the gamma-gamma distribution, $K_\alpha(.)$ represents the modified Bessel function of the second-order α. The parameters α and β are crucial to the model and correspond to the effective number of large-scale

$$\alpha = \left[exp\left[\frac{0.49\,\chi^2}{(1+0.18\,d^2+0.5\,\chi^{12/5})^{7/6}}\right]-1\right]^{-1} \quad (3)$$

$$\beta = \left[exp\left[\frac{0.51\,\chi^2(1+0.69\,\chi^{12/5})^{-5/6}}{(1+0.9d^2+0.62d^2\chi^{12/5})^{7/6}}\right]-1\right]^{-1} \quad (4)$$

where

$$\chi^2 = 0.5\ C_n^2\ k^{7/6} R^{11/6} \quad (5)$$

And $d = (kD_R^2/4R)^{1/2}$ (6)

The parameter $k = 2\pi/\lambda$ is the optical wave number, D_R is the diameter of the receiver collecting lens aperture, R is the link range in metres and C_n^2 is the refractive index structure parameter whose value varies from 10^{-3} $m^{-2/3}$ for strong turbulence to 10^{-17} $m^{-2/3}$ for weak turbulence [16] and small-scale scattering eddies, respectively.

Fisher-Snedecor: This channel model is used to consider strong turbulence having a higher dynamic range. For simulation purposes, m = 3, θ = 2. The PDF of the received irradiance I in this case is expressed as [15]

$$f(I) = \frac{1}{I_o}\ exp\left[-\frac{I}{I_o}\right],\ I \geq 0 \quad (7)$$

where I_o denotes the mean irradiance, the fading parameter $\boldsymbol{\lambda} = \frac{1}{I_o}$. Thus, Equation (7) can be modified to

$$f(I) = \boldsymbol{\lambda}\, exp\,(-\boldsymbol{\lambda}\, I),\ I \geq 0 \quad (8)$$

Negative Exponential: This channel model is used to present deep fading with zero Line of Sight (LOS) rate λ = 1. The PDF of $\mathcal{F}$ is described as [15]

$$f(I) = \frac{2\,m_1^{m_1}\,m_2^{m_2}}{B\,(m_1,\ m_2)} \cdot \frac{I\,m_1^{-1}\,m_2^{m_2}}{(m_1\,I+\ m_2)^{m_1+m_2}} \quad (9)$$

$$B\,(m_1,\ m_2) = \frac{\Gamma(m_1)\,\Gamma(m_2)}{\Gamma(m_1+m_2)} \quad (10)$$

where I is the received optical intensity (irradiance), $I > 0$ m_1 is the degree of freedom parameter (related to turbulence), m_2 is the degree of freedom parameter (related to fading), $B\,(m_1,\ m_2)$ is the beta function and Γ(.) is the Gamma function

Atmospheric datasets (winter, spring, summer, autumn): These datasets have actual real LogCn² values that represent various turbulence conditions observed in nature, the data sets were represented in [11].

Receiver design: based on classical and deep learning algorithms, three receiver architectures have been considered, as shown below:

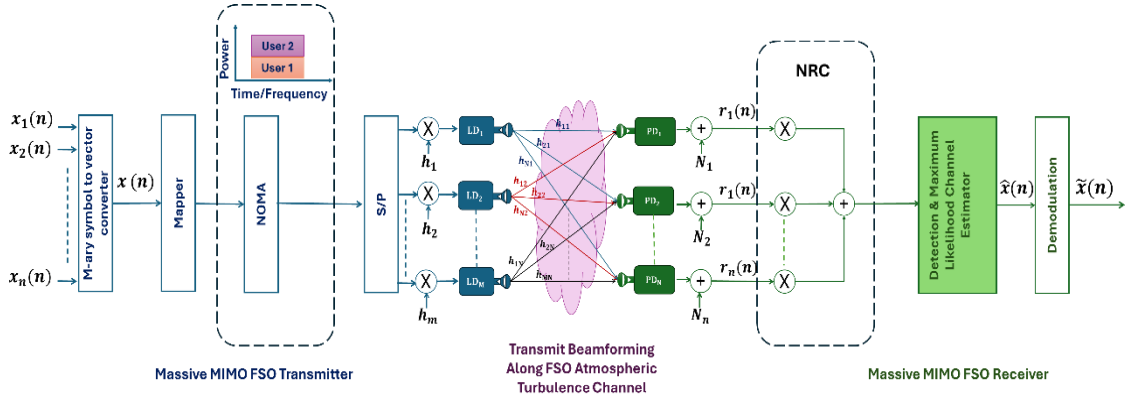

Figure 1. Maximum Likelihood (ML): a conventional detector used as a baseline.

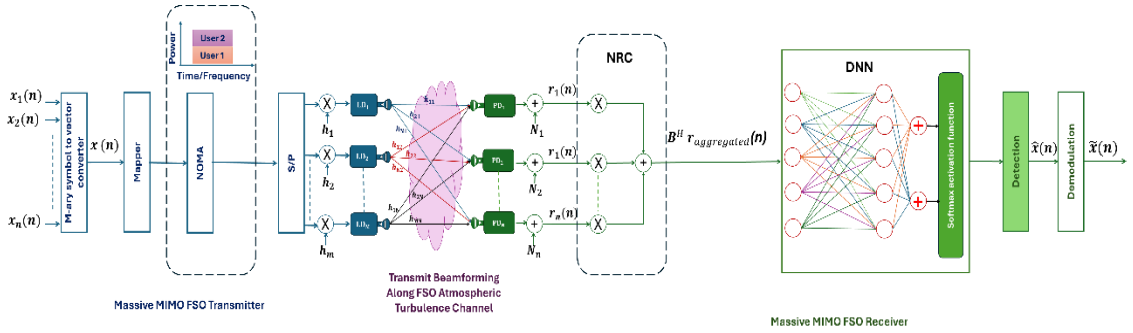

Figure 2. Deep Neural Network (DNN): learns a function from input received signals and channel state to the transmitted symbols

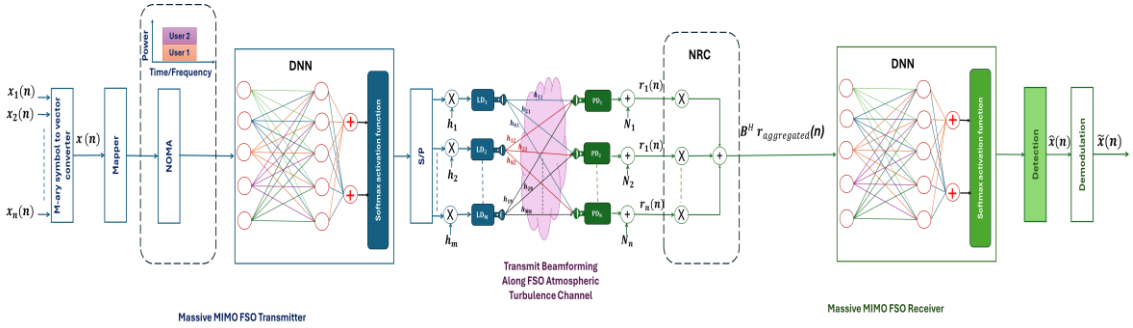

Figure 3. Autoencoder (AE): Jointly learns the transmitter and the receiver using an end-to-end DL model that is capable of robust detection in presence of noise and interference.

Figures 1, 2, and 3 illustrate three different detection approaches for a communication system, each with distinct operating principles and performance characteristics. **Figure 1** shows the *Maximum Likelihood (ML) detector*, a classical baseline method that estimates the transmitted symbols by selecting the sequence most likely to have produced the received signal, given the channel conditions. While ML detection is optimal in minimizing error probability when perfect channel state information is available, it becomes computationally intensive for high-order modulations or large MIMO configurations and is sensitive to channel estimation errors. **Figure 2** presents the *Deep Neural Network (DNN) detector*, a data-driven model that learns the mapping from received signals and channel state directly to transmitted symbols through supervised training. This approach can handle nonlinearities and is generally more robust to imperfect CSI, but it requires substantial training data and may need retraining for varying channel conditions. **Figure 3** illustrates the *Autoencoder (AE)-based end-to-end model*, where the transmitter (encoder) and receiver (decoder) are jointly optimized within a single deep learning framework, with the channel modeled as an intermediate layer. The AE automatically learns optimal modulation, coding, and detection schemes tailored to the channel characteristics, offering improved robustness against noise, interference, and distortions. However, it requires a differentiable channel model during training and can be computationally demanding. Together, these figures demonstrate the evolution from conventional detection to machine learning–driven and fully integrated deep learning solutions, highlighting trade-offs between complexity, adaptability, and performance.

All deep models are trained for a range of SNRs to ensure generalization. The performance of User 1 and User 2 are reported separately to assess the fairness and robustness.

At the transmitter side, the input data d[n] are mapped using QPSK and 16-QAM modulation. The modulated signal is denoted by

$$x[n] = \gamma \sum_{n=1}^{N} \sum_{m=1}^{M} (d_{SB}^{n,m} + I_{DC}) \quad (11)$$

where $d_{SB}^{n,m}$ represents the modulation symbols for the m^{th} laser diode BW_{SB} and n^{th} photodiode detector, and γ is the conversion factor to convert the current to power, where $0 < \gamma \leq 1$.

The constant term I_{DC} in Equation (11) is to ensure the transmitted signal is positive.

However, the optical signal power is denoted by

$$P_{SB}[n] = [0, x_1, x_2, \ldots, x_n, \ldots, \frac{x_{N_{SB}}}{2} - 1, \ldots, 0, \ldots, \frac{x_{N_{SB}}^H}{2} - 1, \quad \ldots, x_2^H, x_1^H]$$

where H represents the Hermitian matrix.

$P_{SB}[n]$ represents the Hermitian symmetry at the output of the NOMA, where it is very important to ensure the optical waveform is transmitted as a non-negative form.

At the channel, the channel matrix for D2D communication is considered as,

$$H_{D2D} = \left[\begin{pmatrix} h_{11} & \cdots & h_{1M} \\ \vdots & \ddots & \vdots \\ h_{N1} & \cdots & h_{NM} \end{pmatrix}_{D_1 D_2}, \ldots, \begin{pmatrix} h_{11} & \cdots & h_{1M} \\ \vdots & \ddots & \vdots \\ h_{N1} & \cdots & h_{NM} \end{pmatrix}_{D_1 D_o} \right] \quad (12)$$

where H_{D2D} is a Device-to-Device (D2D) channel matrix, N is the number of transmission apertures, M is the number of receiver apertures, and h_{nm} is the channel coefficient for the m^{th} laser diode transmitter and the n^{th} photodetector.

At the receiver side, the received signal $\bar{r}(n)$ is denoted by

$$\bar{r}(n) = \mathcal{R}\left[\sum_{n=1}^{N}\sum_{d=1}^{D}\sum_{b=1}^{B}\left[\sqrt{\frac{P_{SB}\rho_D}{P_T M}}\, x[n] \otimes H\right] + n(n)\right] \quad (13)$$

$$\bar{r}_{desired}(n) = \gamma\mathcal{R}\left[\sum_{n=1}^{N}\sum_{m=1}^{M}\sum_{d=1}^{D}\sum_{b=1}^{B}\left[b_i \sqrt{\frac{P_{SB}\rho_D}{P_T M}}\, (d_{SB}^{n,m} + I_{DC}) \otimes H^{(n,m)}\right] + n(n)\right] \quad (14)$$

$$\bar{r}_{interfased}(n) = \gamma\mathcal{R}\left[\sum_{n=1}^{N}\sum_{m=1}^{M}\sum_{d=\bar{d},,\bar{d}\neq 1}^{D}\sum_{b=1}^{B}\left[b_i\ (d_{SB}^{n,m} + I_{DC}) \otimes H^{(n,m)}\right] + n(n)\right] \quad (15)$$

$$\bar{r}_{scattared}(n) = \sum_{S=0}^{S-1}\sum_{N=1}^{N} h(S)\ S(n - T_S) \quad (16)$$

$$\bar{r}_{aggregated}(n) = \bar{r}_{desired}(n) + \bar{r}_{interfased}(n) + \bar{r}_{scattared}(n) + \bar{N}(n) \quad (17)$$

where

$\mathcal{R}[.]$ is the operator's real part (may be used to ensure the optical signal is real-valued) and P_{SB} is the power allocated per sub-band.

P_T is the total transmitted power.

D is the number of devices per sub-band (NOMA users).

$x[n]$ is the transmitted symbol vector at time n.

$\otimes$ represents convolution (matrix operation).

H is the channel matrix (includes turbulence, pointing error, etc.).

$n(n)$ is the additive white Gaussian noise (AWGN).

$h(S)$ represents the scattering channel response,

S is the signal transmitted by the scatterers,

T_S is the time delay

the aggregated received signals can be modeled as

$$\bar{r}(n) = H\,\bar{x}(n) + \bar{N}(n) \quad (18)$$

$$H^{-1}\,\bar{r}(n) = \bar{x}(n) + H^{-1}\,\bar{N}(n) \quad (19)$$

$$error = \|\bar{r}(n) - H\,\bar{x}(n)\|^2 \quad (20)$$

The estimated transmitted vector is thus

$$\bar{x}(n) = (H^H H)^{-1} H^H\,\bar{r}(n) \quad (21)$$

Simplified into parallel data paths using Singular Value Decomposition (SVD) such that $H = U\sum V^H$ this simplification of the MIMO detection process into orthogonal channels which makes linear receivers, such as Zero-Forcing (ZF) or the Minimum Mean Square Error (MMSE), more efficient.

$$\begin{bmatrix}\tilde{r}_1(n)\\ \tilde{r}_2(n)\\ \vdots\\ \tilde{r}_m(n)\end{bmatrix} = \begin{bmatrix}\sigma_1 & 0 & \dots & 0\\ 0 & \sigma_1 & \dots & 0\\ \vdots & \vdots & \ddots & \vdots\\ 0 & 0 & \dots & \sigma_m\end{bmatrix}\begin{bmatrix}\tilde{X}_1(n)\\ \tilde{X}_2(n)\\ \vdots\\ \tilde{X}_m(n)\end{bmatrix} + \begin{bmatrix}\widetilde{N}_1(n)\\ \widetilde{N}_2(n)\\ \vdots\\ \widetilde{N}_m(n)\end{bmatrix} \quad (22)$$

Where $\tilde{r}\ \ (n)$ is the estimated received symbol, the above equation can be rewritten as

$$\begin{aligned}\tilde{r}_1(n) &= \sigma_1\,\tilde{X}_1(n) + \widetilde{N}_1(n)\\ \tilde{r}_2(n) &= \sigma_2\,\tilde{X}_1(n) + \widetilde{N}_2(n)\\ &\vdots\\ \tilde{r}_m(n) &= \sigma_m\,\tilde{X}_m(n) + \widetilde{N}_m(n)\end{aligned} \quad (23)$$

To compute the SINR at the beamformers output, the signal and noise powers must be computed such that

$$\bar{B}_1^*\,\bar{r}_1(n) + \bar{B}_2^*\,\bar{r}_2(n) + \dots + \bar{B}_n^*\,\bar{r}_n(n) \quad (24)$$

The above formula can be denoted in matrix form:

$$[\bar{B}_1^* \quad \bar{B}_2^* \quad \dots \quad \bar{B}_n^*]\begin{bmatrix}\bar{r}_1(n)\\ \bar{r}_2(n)\\ \vdots\\ \bar{r}_n(n)\end{bmatrix} = \bar{B}^H\,\bar{r}_{aggregate}(n) \quad (25)$$

Then, the beamformer output is

$$\bar{B}^H\left(\sqrt{\frac{P_{SB}\rho_D}{P_T M}}\,\bar{H}\,\bar{x}(n) + \bar{N}(n)\right)$$

$$\bar{B}^H\sqrt{\frac{P_{SB}\rho_D}{P_T M}}\,\bar{H}\,\bar{x}(n) + \bar{B}^H\,\bar{N}(n) \quad (26)$$

From the equation above, the signal power is computed using

$$P_{Signal} = \sqrt{\frac{P_{SB}\rho_D}{P_T M}}\,\left|\bar{B}^H\,\bar{H}\right|^2.P_{Transmitted} \quad (27)$$

The noise power at the beamformer output can be computed using

$$\mathbb{E}\{\bar{N}(n)\quad \bar{N}^H(n)\} = \mathbb{E}\left\{\begin{bmatrix}N_1(n)\\ N_2(n)\\ \vdots\\ N_n(n)\end{bmatrix}[N_1^*(n) \quad N_2^*(n) \quad \dots \quad N_n^*(n)]\right\} \quad (28)$$

where $\mathbb{E}[.]$ represents the expectation operator.

$$\mathbb{E}\{\bar{N}(n)\quad \bar{N}^H(n)\} = \begin{Bmatrix}N_1(n)N_1^*(n) & N_1(n)N_2^*(n) & \dots & N_1(n)N_n^*(n)\\ N_2(n)N_1^*(n) & N_1(n)N_2^*(n) & \dots & N_2(n)N_n^*(n)\\ \vdots & \vdots & \ddots & \vdots\\ N_n(n)N_1^*(n) & N_n(n)N_2^*(n) & \dots & N_n(n)N_n^*(n)\end{Bmatrix} \quad (29)$$

$$\mathbb{E}\{\bar{N}(n)\quad \bar{N}^H(n)\} = \begin{Bmatrix}\sigma_N^2 & 0 & \dots & 0\\ 0 & \sigma_N^2 & \dots & 0\\ \vdots & \vdots & \ddots & \vdots\\ 0 & 0 & \dots & \sigma_N^2\end{Bmatrix} \quad (30)$$

$$\mathbb{E}\{\bar{N}(n)\quad \bar{N}^H(n)\} = \sigma_N^2\,I \quad (31)$$

$$Noise\ power = \mathbb{E}\{[\bar{B}^H\,\bar{N}(n)]\quad [\bar{B}\,\bar{N}^H(n)]\} \quad (32)$$

$$Noise\ power = \bar{B}^H\,\bar{B}\,\mathbb{E}\{\bar{N}(n)\,\bar{N}^H(n)\} \quad (33)$$

$$Noise\ power = \sigma_n^2\,\|\bar{B}\|^2 \quad (34)$$

Equation (34) represents the noise power at the beamformer, where the SINR is denoted as

$$SINR = \left[\frac{\sqrt{\frac{P_{SB}\rho_D}{P_T M}}\left|\bar{B}^H H\right|^2 P_{Transmitted}}{\gamma\mathcal{R}\left[\sum_{n=1}^{N}\sum_{m=1}^{M}\sum_{d=\bar{d}}^{D}\sum_{b=1}^{B}\left|\bar{B}^H H\right|^2 P_{Transmitted} + \sum_{S=0}^{S-1}\sum_{M=0}^{M-1}|h(S)|^2 P_{Scattered} + \sigma_n^2\,\|\bar{B}\|^2\right]}\right] \quad (35)$$

3. Deep Learning Process

Channel Estimator DNN Architectures for QPSK

The proposed DNN-based channel estimators are designed for the QPSK modulation format, in which the input feature to the neural network is the atmospheric turbulence parameter $LogCn^2$ indicating the level of channel fading experienced due to turbulence. The same DNN architecture is modified to suit different fading dynamics by simply adjusting the number of hidden layers and the number of neurons in each layer as detailed below.

The regression output layer of the DNN for QPSK would consist of two neurons for the real and imaginary parts of the complex channel gain to estimate the in-phase (I) and quadrature (Q) components of the channel gains for real and imaginary parts. The non-linearity function used for all hidden layers is ReLU.

End-to-end autoencoder architecture for QPSK symbol recovery

An end-to-end autoencoder (AE) framework is setup in which the modulation and demodulation components can be jointly optimized for a QPSK-based FSO system. In the transmitter, i.e., the encoder, input symbols are one-hot encoded and passed through a compact AE architecture consisting of three layers (128→64→2 neurons), with the last layer encoding for the real and imaginary parts of the QPSK-modulated symbol.

The receiver, i.e., the decoder, has the noisy received symbols along with the corresponding channel gains as the input. The autoencoder decoder processes these through two hidden layers with 64→128 neurons, which is then followed by a Softmax output layer that classifies and recovers the transmitted symbols. The above encoder–decoder framework can be viewed as a fully trainable communication pipeline with optimal mappings that are learned based on the actual channel. A learning-based communication architecture like the one above is particularly useful for FSO systems, where the channel characteristics change rapidly and are difficult to model with an analytical expression. The autoencoder framework can learn to adapt to such rapid changes and aid in robust symbol detection for different turbulence levels.

4. Simulation Parameters and Results

The simulation setup employs QPSK modulation scheme under various channel models, including Log-Normal ($\sigma = 0.3$), Gamma–Gamma ($\alpha = 3.0$, $\beta = 2.0$), Negative Exponential ($\lambda = 1.0$), Fisher–Snedecor ($m = 3.0$, $\theta = 2.0$), and real-world atmospheric channels derived from measured datasets [11]. The system experiences additive white Gaussian noise (AWGN) and utilizes direct detection with maximum ratio combining (MRC) as the receiver model. The photodetector responsivity is set to 1. For the NOMA configuration, User 1 and User 2 are assigned power coefficients of 0.8 and 0.2, respectively. The simulations are implemented using Python 3.x with libraries such as NumPy, SciPy, Matplotlib, and TensorFlow.

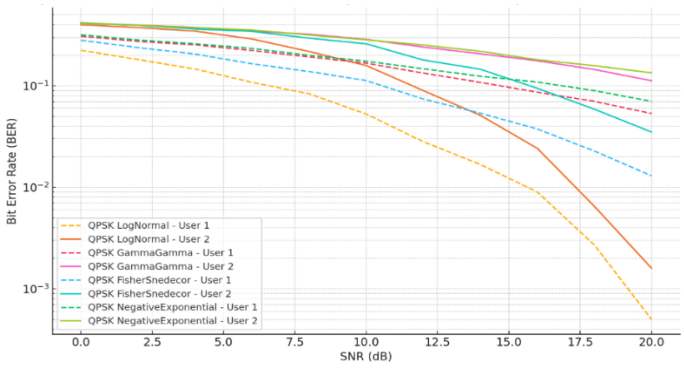

Figure 4. BER vs SNR for 64X64 MIMO FSO NOMA for 2 users, QPSK with 4 impirical channel model

Figure (4) depicts the BER versus SNR curves of the two users (User 1 and User 2) for the QPSK modulation using 64×64 MIMO-FSO-NOMA. In this simulation, four channel models (Log-Normal, Gamma-Gamma, Fisher-Snedecor, and Negative Exponential) are considered. It can be seen that the Log-Normal and Gamma-Gamma channels outperform the others, especially for User 1 in terms of BER. This implies that the Log-Normal and Gamma-Gamma channels are more resilient against moderate turbulence. In contrast, the worst case is when the Negative Exponential channel is considered, due to the worst fading characteristics and lack of diversity. As observed, User 1 performs better than User 2, as expected. However, this difference is significantly higher in the case of severe fading, which means that the conventional SIC method fails to cope with a weak user. To overcome this issue, machine learning can be integrated to ensure reliable communication of weak users in adverse conditions.

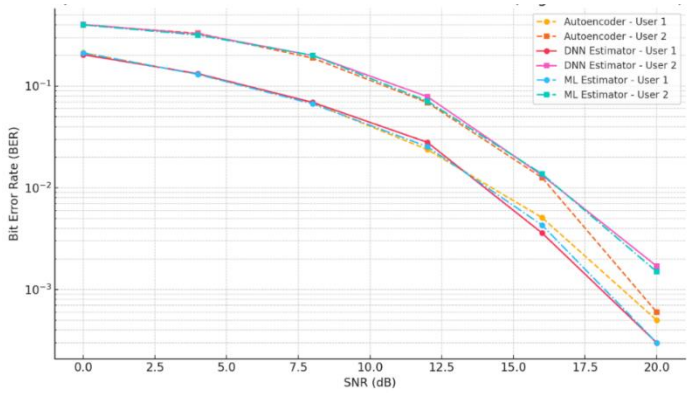

Figure 5. BER vs SNR for 64X64 MIMO FSO NOMA for 2 users, QPSK with Log Normal channel model and DNN design structure

The figure (5) above shows BER versus SNR performance comparison between three detection schemes (deep autoencoder based end-to-end, deep neural network (DNN) based channel estimator and maximum likelihood (ML) based channel estimator) in 64×64 MIMO-FSO NOMA system using QPSK modulation in Log-Normal turbulence channel. The BER of both users is depicted for all methods. For both users, the best performance is achieved by the autoencoder based system due to the autoencoder learning the optimal mapping that compensate for the combined effect of interference and turbulence. Similarly, for both users, DNN based channel estimator achieves better performance compared to the conventional ML based channel estimator due to DNN learning the channel statistics and making the symbol recovery more accurate. Also, User 1 always performs better than User 2 for all the methods since the NOMA grants the User 1 more power.

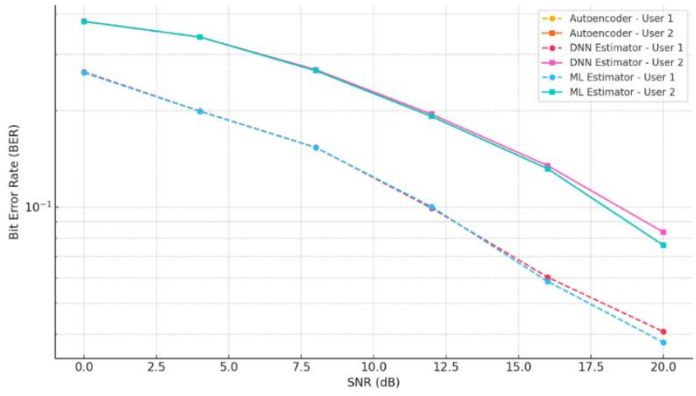

Figure 6. BER vs SNR for 64X64 MIMO FSO NOMA for 2 users, QPSK with Gamma-Gamma channel model and DNN design structure

Figure (6) illustrates the BER versus SNR for the 64X64 MIMO-FSO NOMA system using QPSK for both users with three receiver techniques, namely, an autoencoder-based DL model, a DNN-based channel estimator, and the ML estimator for both User 1 and User 2. It can be seen that all three estimators have comparable BER performance for both users, and the NOMA scheme enhances the performance for User 2 more than that for User 1. In fact, the improvement in BER for User 2 compared to that of User 1 is much larger for the DNN estimator compared to the ML estimator. In the low SNR region, the ML estimator results in a large reduction in BER for User 2, whereas the autoencoder-based DL model and the DNN-based channel estimator do not have a significant impact on BER. This is because of the Gamma-Gamma model, which can introduce significant fading. Due to the combined small-scale and large-scale fading, the Gamma-Gamma channel model causes difficulties in estimation. In this case, autoencoder-based DL models and DNN-based channel estimators provide better BER performance compared to ML.

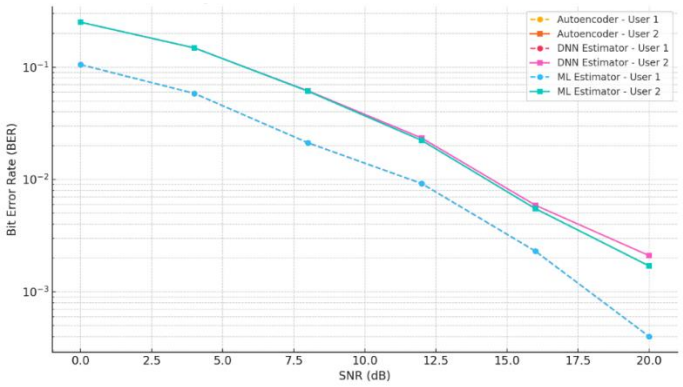

Figure 7. BER vs SNR for 64X64 MIMO FSO NOMA for 2 users, QPSK with Fisher-Snedecor channel model and DNN design structure

Figure (7) compares the BER performance of 64X64 MIMO-FSO NOMA system for QPSK modulation using three receivers: autoencoder-based deep learning, DNN-based channel estimator, and maximum likelihood (ML) estimator over Fisher-Snedecor channel model. Fisher-Snedecor channel model is suitable to simulate strong fading channel and model different channel conditions. It can be observed that autoencoder and DNN have similar BER performance for User 1 and User 2. In addition, the BER performance of both users has good performance at high SNR. It is worth noting that the BER performance of ML has a significant degradation for User 2 due to its inability to suppress nonlinear interference and fading. The simulation results have proven that deep learning has the advantage to accommodate the channel environment and consistent gain for User 1 due to higher power in NOMA.

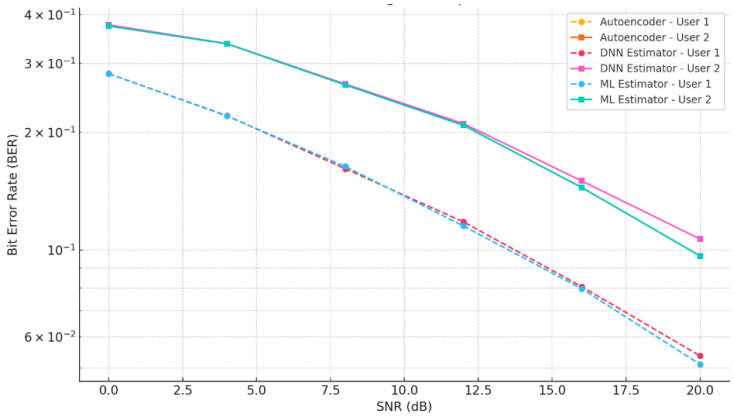

Figure 8. BER vs SNR for 64X64 MIMO FSO NOMA for 2 users, QPSK with Negative Exponential channel model and DNN design structure

The figure (8) shows the BER versus SNR curves of the proposed system using QPSK modulation under a Negative Exponential turbulence channel model. It is worth noting that this is the worst case of the considered channel models as it corresponds to severe atmospheric turbulence without line-of-sight scatter. We can observe the performance of three schemes; the autoencoder based deep learning, the DNN based channel estimator, and the conventional ML scheme for both users. We can observe that the performances of the deep learning based algorithms (autoencoder and DNN) are better than ML for both users. Nevertheless, in the harsh case of severe turbulence conditions, the achieved BER is high even at 20 dB for User 2. This shows the failure of classical SIC and ML estimators.

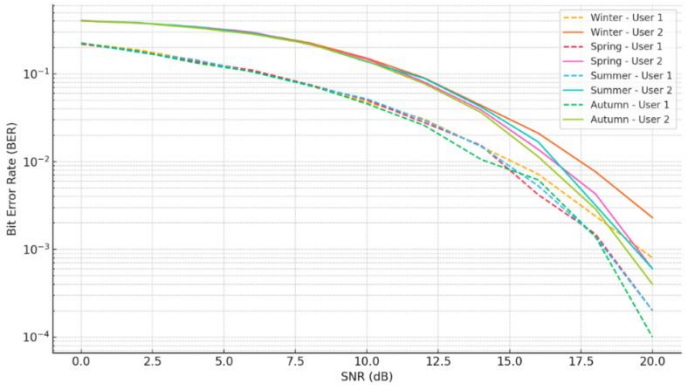

Figure 9. BER vs. SNR for Massive MIMO FSO NOMA for 2 users; QPSK with seasonal channel dataset model and DNN design structure.

Figure (9) shows the BER versus SNR for the Massive MIMO-FSO NOMA system with QPSK modulation using the real atmospheric turbulence data obtained in winter, spring, summer, and autumn. The performance of the system in terms of BER for User 1 and User 2 for different seasons with $\log Cn^2$ turbulence strength (obtained from real environmental parameters) were compared. According to the analysis, as mentioned earlier, User 1 had a better BER than User 2 in all cases because of the higher power allocation for User 1. Furthermore, in the cases of summer and autumn, the overall BERs for Users 1 and 2 were less in comparison with those in winter and spring. In summer and autumn, the BER values for Users 1 and 2 were comparatively stable. This might have happened due to the lower variation in atmospheric turbulence in summer and autumn compared with winter and spring. In addition, in the cases of winter and spring, there was more degradation in the BER for User 2 compared with summer and autumn for low and medium SNR values.

6. Conclusion

In this paper, the BER performances of an autoencoder receiver have been shown for 64x64 MIMO-FSO NOMA system with QPSK modulation in four theoretical and four realistic seasonal channels. The simulation results reveal that deep learning-based receiver outperforms conventional ML-based estimators for NOMA users in all four theoretical and four seasonal realistic FSO channels. Therefore, it is possible to conclude that the proposed NOMA-aided system, which works in moderate fading as well as in severe fading conditions, can be used in real-time communication systems in future generations of FSO systems.

Funding: "This research received no specific grant from funding agencies in the public, commercial, or not-for-profit sectors. All expenses were covered by the authors' affiliated institutions."

Conflicts of Interest: "The authors declare that there are no known financial or personal conflicts of interest that could have appeared to influence the work reported in this paper."

References

[1] Kumar, R. G. Sangeetha, and M. P. Sharma, "Advanced techniques for enhancing free space optical communication systems under varying atmospheric conditions," *Journal of Optical Communications*, vol. 45, no. 3, pp. 123–134, 2023.

[2] M. A. Atiyah, L. F. Abdulameer, and G. Narkhedel, "PDF comparison based on various FSO channel models under different atmospheric turbulence," *Al-Khwarizmi Engineering Journal*, vol. 19, no. 4, pp. 78–89, 2023.

[3] H. F. Radeef, L. F. Abdulameer, and H. M. Fadhil, "Machine learning for free space optical communication: A systematic review with emphasis on NOMA and massive MIMO integration," *Fusion: Practice and Applications*, vol. 20, no. 2, pp. 65–76, 2025.

[4] D. A. Kumar and R. G. Sangeetha, "Power series based gamma–gamma fading MIMO/FSO link analysis with atmospheric turbulence and pointing errors," *Optical and Quantum Electronics*, vol. 53, no. 505, 2021.

[5] M. A. Esmail *et al.*, “Free space optic channel monitoring using machine learning,” *Optics Express*, vol. 29, pp. 10967–10981, 2021.

[6] L. J. S. Kumar, P. Krishnan, B. Shreya, and S. M. S. M., “Performance enhancement of FSO communication system using machine learning for 5G/6G and IoT applications,” *Optik*, vol. 252, Art. no. 168430, 2022.

[7] M. P. Bart *et al.*, “Deep learning for enhanced free-space optical communications,” *arXiv: 2208.07712*, 2022.

[8] S. A. Abd El-Mottaleb *et al.*, “Machine learning FSO-SAC-OCDMA code recognition under different weather conditions,” *Optical and Quantum Electronics*, vol. 54, p. 851, 2022.

[9] S. Henna, A. A. Minhas, M. S. Khan, and M. S. Iqbal, “Ensemble consensus representation deep reinforcement learning for hybrid FSO/RF communication systems,” *Optics Communications*, vol. 530, Art. no. 129186, 2023.

[10] M. A. Esmail, “Performance monitoring of hybrid all-optical fiber/FSO communication systems,” *Applied Sciences*, vol. 13, no. 14, p. 8477, 2023.

[11] Lionis *et al.*, “Experimental machine learning approach for optical turbulence and FSO outage performance modeling,” *Electronics*, vol. 12, no. 3, p. 506, 2023.

[12] S. A. A. El-Mottaleb, A. Elhefny, A. Métwalli *et al.*, “Harnessing the power of ML for robust SISO and MIMO FSO communication systems in fog weather,” *Optical and Quantum Electronics*, vol. 56, p. 1065, 2024.

[13] M. S. N. Al-Imran, H. Nguyen, and Y. M. Jang, “Channel estimation of massive MIMO FSO communication system using deep attention residual U-Net,” *ICT Express*, 2024.

[14] P. A. Forsido, D. J. Gelmecha, and R. S. Singh, “Machine learning–based multiparameter performance predictions of ultra-dense WDM FSO–FTTx systems under diverse weather conditions,” *International Journal of Optics*, vol. 2025, Art. no. 6697110, 2025.

[15] H. Kaushal, V. K. Jain, and S. Kar, “Free-space optical channel models,” in *Free Space Optical Communication*, New Delhi, India: Springer, 2017, ch. 2, pp. 41–89.

[16] D. Benton, Y. Li, A. Billaud, and A. D. Ellis, “Spatial mode division multiplexing of free-space optical communications using a pair of multiplane light converters and a micromirror array for turbulence emulation,” *Photonics*, vol. 11, no. 3, art. 241, 2024.